INTERNATIONAL JOURNAL FOR NUMERICAL METHODS IN FLUIDS, VOL. 23, 295–306 (1996)

NUMERICAL PREDICTION OF SEMI-CONFINED JET IMPINGEMENT AND COMPARISON WITH EXPERIMENTAL DATA

S. ASHFORTH-FROST AND K. JAMBUNATHAN

Department of Mechanical Engineering, The Nottingham Trent University, Nottingham NG1 4BU, U.K.

SUMMARY

The standard k–ε eddy viscosity model of turbulence in conjunction with the logarithmic law of the wall has been applied to the prediction of a fully developed turbulent axisymmetric jet impinging within a semi-confined space. A single geometry with a Reynolds number of 20,000 and a nozzle-to-plate spacing of two diameters has been considered with inlet boundary conditions based on measured profiles of velocity and turbulence. Velocity, turbulence and heat transfer data have been obtained using laser–Doppler anemometry and liquid crystal thermography respectively. In the developing wall jet, numerical results of heat transfer compare to within 20% of experiment where isotropy prevails and the trends in turbulent kinetic energy are predicted. However, stagnation point heat transfer is overpredicted by about 300%, which is attributed directly to the turbulence model and inapplicability of the wall function.

KEY WORDS: impinging jet; turbulence; heat transfer; k–ε model

1. INTRODUCTION

Jet impingment flows are frequently used in industrial practice for their high heat and mass transfer rates. Their employment is common but also diverse and typical applications include many heating, cooling and drying processes such as the manufacture of printed wiring boards, printing processes, production of foodstuffs, de-icing of aircraft wings and cooling of turbine aerofoils. The high heat transfer rates are especially needed to achieve short processing times for product quality or owing to temporal limitations of the process and/or for energy efficiency.

The fluid dynamic structure of such processes is extremely complex and as such it is often reduced to that of understanding a single impinging jet, which will be turbulent except at very low Reynolds numbers. Even when the practical application is simplified, the necessary experimental rigs can be cumbersome and expensive, not to mention the time-consuming data acquisition, validation and analysis. Numerical simulations are an alternative to the experimental approach and can provide a fast and economic solution which will describe the flow or at least identify trends in the flow or heat transfer distribution. In this case the designer needs to be aware of the reliability and limitations of the numerical solutions for that particular geometry under investigation. An assessment of the model can only be obtained by comparison with experiment. Since numerical solutions are problem-dependent, there is a need for reliable experimental data specific to the jet impingement geometry to facilitate a direct assessment.

CCC 0271–2091/96/030295–12

Received July 1995
Revised December 1995

Both the $k-\varepsilon$ model and Reynolds stress models have predicted a wide variety of flows to reasonable accuracy. However, the use of the $k-\varepsilon$ turbulence model in jet impingement is not entirely justified, since, as will be shown in this study, the impinging jet is anisotropic and the basic assumption of the $k-\varepsilon$ model, which employs the Boussinesq hypothesis, is local isotropy. In flows with normal straining, the $k-\varepsilon$ model predicts a high generation rate of turbulence,[1] which can cause an overprediction of skin friction coefficients and thus heat transfer. Despite the expectation that the Reynolds stress models would improve the prediction of impinging flows, evidence to date reveals that this only happens when specific near-wall models are used,[1] which at present are not widely available. Consequently, the $k-\varepsilon$ model is most often adopted owing to its simplicity and economy over the second-moment closure models. This, combined with the fact that the $k-\varepsilon$ model was available for several years before the Reynolds stress models, has resulted in it being adopted as a standard option in many commercial packages and its subsequent frequent use in both academia and industry.

Jet impingement is a broad topic and there is consequently an extensive amount of archived literature including theoretical, experimental and numerical works. There are many variable quantities and several reviews on the subject are available. These range from comprehensive lists of publications arranged in chronological order[2–4] or classified into various categories[5–11] to succinct critical reviews.[12] Numerical works on flow and heat transfer characteristics of jet impingement have been reviewed by Polat *et al.*[11] The numerical errors associated with some of the early simulations cited prevent any reliable assessment of the turbulence model accuracy. In the last 5 years the importance of the jet impingement flow field has led to liaison between a number of experimental and numerical research teams from both industry and academia.[13] The unconfined impinging jet geometry has been adopted as a vehicle for comparison of various turbulence models and computational packages with experimental results at $Re \approx 23{,}000$ and $z/d = 2$. Upper entrainment boundary conditions were approximated. Several workers experienced problems with convergence due to this entrainment boundary and modified the conditions so as to attain convergence. Results[14,15] obtained using the standard $k-\varepsilon$ and Reynolds stress models were compared with experimental results of heat transfer distribution[16] and some velocity and turbulence results[17] within the stagnation region. Numerical resolution was considered satisfactory, but variations between model/model and model/experiment were still evident. The variations could be partly attributed to the treatment of the entrainment boundary and different solution algorithms employed. The most promising results were obtained using a Reynolds stress model with a new wall reflection model.[18] However, this model is in the early stages of development and its generality is as yet unknown. In a more recent contribution,[19] predictions are compared with experimental results from the same laboratory.[17] The $k-\varepsilon$ model was shown to overpredict the heat transfer coefficient due to unconfined jet impingement, which was attributed to the overprediction of the turbulent kinetic energy near the stagnation point.

Attempts to assess the relative merits of various computational approaches have been hindered by the lack of detailed experimental data and the varied specification of the flow field boundaries. Ideally, the same boundary conditions should be used for each case so that the differences can be linked directly to the numerical model. In this paper, experimentally measured boundary conditions are specified at the jet exit. A semi-confined configuration was selected because, despite the industrial relevance of this geometry, very few works were identified in the existing literature[12,20] and the upper solid boundary simplifies the specification of the problem numerically, facilitating a direct assessment of the model under investigation.

2. EXPERIMENTAL INVESTIGATION

Details of the experimental facilities and procedures can be found in Reference 21. Uncertainties have been estimated using established techniques.[22] A 10 mW single-component laser–Doppler anemometry system (DANTEC 55X) was used to obtain mean velocity and turbulence data. A local frequency shift

was applied to one of the system beams to provide directional sensitivity. A 3 × beam expander reduced the diameter of the measurement volume to 1·2% of the nozzle diameter, and by using an off-axis arrangement for light collection, the effective length of the measurement volume was reduced to 3·75% of the nozzle diameter. A microcomputer-controlled two-dimensional traverse mechanism and instrumentation system facilitated automatic and random data acquisition. The frequency tracker processor required continuous seeding, which was provided by olive oil particles from a seeding generator. To avoid uneven particle concentrations leading to biased measurements, the jet arrangement was enclosed in a large chamber to ensure seeding of the entrained air. Overall uncertainties in the mean velocity and turbulence intensity are estimated to be 4% and 5% respectively. The uncertainties in the axial, radial and transverse radial directions due to initial positioning of the measurement volume are estimated to be 25% of the measurement volume dimensions. Nearly 30% of all measurements were repeated and were found to be repeatable within the uncertainty intervals, except very close to the impingement wall and in the shear layer region. Uncertainty in these regions is evident from the scatter in the results presented and is attributed to the finite length of the measurement volume and near-wall reflections.

The distribution of Nusselt number was obtained using a transient wall-heating technique that requires the measurement of the elapsed time to increase the temperature of the liquid-crystal-coated impingement plate to a predetermined value. The rate of heating was recorded by monitoring the colour change patterns of the liquid crystal with respect to time as the hot air jet impinged onto the plate. The heat transfer process was considered to be one-dimensional into a semi-infinite medium, since the test specimen was sufficiently thick and of low thermal diffusivity. An exact solution to the one-dimensional transient conduction equation then yielded the heat transfer coefficient. The uncertainty in the measured heat transfer coefficient is estimated to be less than 8%.

3. NUMERICAL INVESTIGATION

3.1. The solution procedure

Detailed descriptions of the most common discretization procedures, convection–diffusion schemes and solution algorithms are provided in several texts.[23–26] In this investigation the computations were carried out using PHOENICS 1.6.2. The solution procedure is based on a finite volume discretization, on a staggered grid, of the governing equations of heat, mass and momenum.[27] A hybrid upwind interpolation scheme was specified to handle the combined effects of convection and diffusion, but in practice the upwind scheme is activated over most of the flow domain. PHOENICS uses the SIMPLEST (semi-implicit method for pressure-linked equations shortened) solution algorithm to enforce continuity and solves the discretised equations iteratively using the TDMA (tridiagonal matrix algorithm) line solver.[23] Owing to the curvature of the flow, the whole field solution procedure was implemented.

The standard high-Reynolds-number version of the k–ε model has been employed in this investigation. The turbulence model constants used have given good agreement with a range of free turbulent flows and wall flows[28] and have the following standard values:[29] $\sigma_k = 1{\cdot}0$, $\sigma_\varepsilon = 1{\cdot}3$, $C_\mu = 0{\cdot}09$, $C_1 = 1{\cdot}44$ and $C_2 = 1{\cdot}92$.

In the immediate vicinity of the impingement and upper confinement plates where the local Reynolds number is low, viscous effects are influential, so a wall function is used to bridge this area. The logarithmic law of the wall was used to compute the skin friction factor, which is used to determine the Stanton number. For turbulent flow this assumes a logarithmic dependence of the radial velocity on the normal co-ordinate to the wall and that the production of turbulent kinetic energy is equal to the dissipation in the log-law region. The implementation of this wall function into PHOENICS is described

by Rosten and Worrell[30] and in further detail by Ludwig *et al.*[26] Skin friction, Stanton number and other computed variables were extracted from PHOENICS during its execution by using appropriate GROUND coding.[21] When the local Reynolds number $Re > 132{\cdot}5$, the skin friction is given by

$$s = \left(\frac{\kappa}{\ln(1{\cdot}01 + 9\,Re\,s^{0{\cdot}5})}\right)^2, \tag{1}$$

where κ is the von Karman constant and the local Reynolds number Re is defined as

$$Re = y_p v_p / \nu. \tag{2}$$

Otherwise

$$s = 1/Re. \tag{3}$$

The Stanton number is then computed from

$$St = s/\sigma_t(1 + Ps^{0{\cdot}5}), \tag{4}$$

where

$$P = 9\left(\frac{\sigma_l}{\sigma_t} - 1\right)\left(\frac{\sigma_t}{\sigma_l}\right)^{0{\cdot}25}. \tag{5}$$

The development of this equation is described by Jayatilleke.[31] Values of the laminar and turbulent Prandtl numbers σ_l and σ_t of 0·7 and 0·9 for air were specified. The Stanton number is based on the enthalpies at the near-wall node and at the wall and is used to obtain the heat flux to the wall via

$$St = -\dot{q}/(h_p - h_w)\rho v_p. \tag{6}$$

3.2. *The grid*

An axisymmetric polar grid was used with the z-axis aligned with the nozzle centreline and the y-axis being radial. The effect of the length of the solution domain was examined to ensure that the outflow boundary did not lie within a recirculation region. As a result, the impingement and confinement plates were extended to $15d$. Nodes were concentrated in regions of large gradients; namely, close to the impingement surface and at the edge of the jet (shear layer). Based on a grid dependence study,[21] a 100×68 grid was adopted, shown in Figure 1. For the area between the wall and the near-wall node, k and ε are obtained from the wall function which requires the near-wall node to lie just inside the turbulent region. In this case a near-wall cell size of $0{\cdot}02d$ was adopted, guided by experiment, which corresponds to a near-wall Reynolds number greater than 132 ($y^+ > 11{\cdot}5$).

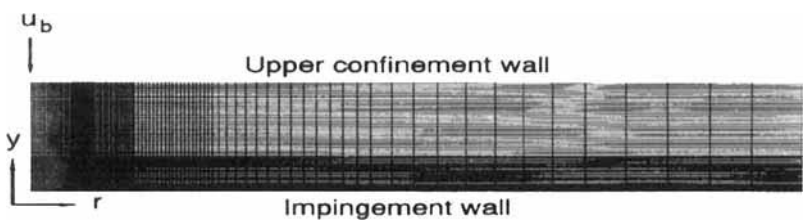

Figure 1. 100×68 grid, $z/d = 2, r/d = 15$

3.3. *Boundary conditions*

The elliptic nature of the flow field requires that the boundary conditions be specified on all sides of the solution domain. Measured values of velocity and turbulence intensity, obtained using laser–Doppler anemometry at the exit plane of a $20d$ sharp-edged nozzle, were specified at the jet exit. These inlet conditions represent a fully developed velocity profile and are presented in Figure 2. The dissipation was deduced from[26] $\varepsilon = C_\mu^{3/4} k^{3/2}/L$, where L was estimated to be 5% of the inlet diameter. Zero velocities were specified at the solid surfaces and a logarithmic wall function was activated. A floating zero pressure was specified at the outlet boundary and the computed pressure is relative to it. The use of the PHOENICS Input Language (PIL) command SAME ensured that any inflowing mass brings in the same value of the variable as already prevails in the cell. A constant temperature was prescribed at the wall, which simulates the experimental boundary condition. Viscosity, thermal conductivity, specific heat and density were modelled as being independent of temperature.

3.4. *Convergence*

To assist convergence, the pressure and velocity fields were solved to provide reasonable initial fields before activating the k–ε turbulence model. Linear and false time step underrelaxation were also applied to pressure and the other variables respectively to help procure convergence. Relaxation was not applied to the enthalpy equation, since the temperature changes are small enough so as not to contribute any significant effect to the transport properties. In addition, the enthalpy equation was only solved when convergence of the other variables had been achieved. The amount of relaxation varied as the solution progressed (pressure: 0·8–0·2; velocities and other scalars: locally dependent on grid size and in-cell value), the greater relaxation being applied to the turbulent quantities. Only when local relaxation was applied to the velocity and turbulent quantities was a converged solution achieved. The local values of false time step were obtained by dividing a characteristic length by a characteristic velocity. For the velocities the cell size and local velocity were used, whereas for the turbulent kinetic energy the turbulent kinetic energy divided by the energy dissipation rate was used. Maximum and minimum values for the variables and initial values were also specified according to the jet inlet conditions. The sums of the absolute residuals of the continuity and momentum equations were used to monitor convergence.

Typically 2500 sweeps were necessary to procure convergence, which used approximately 2 h CPU time on the VAX 4600 computer.

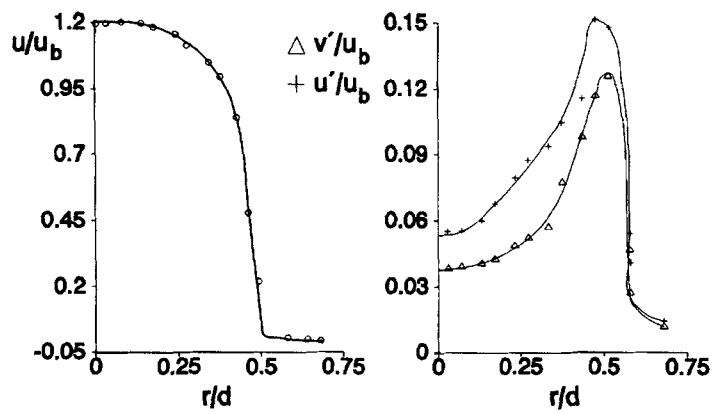

Figure 2. Specified inlet boundary conditions

4. PRESENTATION AND DISCUSSION OF RESULTS

4.1. Velocity and turbulence profiles

Cooper *et al.*[17] reviewed the work of several research groups who have used the k–ε eddy viscosity model for unconfined jet impingement at $z/d = 2$ and $Re = 23{,}000$. The present results for semi-confined impingement are consistent with the envelope of these predictions, shown in Figure 3.

Numerical and experimental profiles of radial velocity are compared in Figure 4. The first graph also presents the axial velocity profile, which shows good agreement with experiment. The correct trends in the radial velocity profiles are predicted, in that the radial velocity develops to a maximum at $r/d \approx 1$, reducing in magnitude as the wall jet develops. The near-zero radial velocities above the wall jet ($y/d > 0{\cdot}75$) are also fairly predicted. However, the spreading rate is underpredicted at all radial stations (maximum velocities underpredicted by 12% at $r/d = 0{\cdot}5$, 25% at $r/d = 1$ and 40% at $r/d = 2$). At the edge of the jet, $r/d = 0{\cdot}5$, the computed profile compares reasonably well with experiment, but as the jet develops further, the wall jet becomes too thick. For $r/d \geqslant 2$ the predicted profiles improve progressively with radial distance.

Numerical and experimental profiles of turbulent kinetic energy are compared in Figure 5. The correct trends in the development of the turbulent kinetic energy k are predicted when $r/d \geqslant 1$, and when $y/d > 0{\cdot}75$, the magnitudes of k are also well predicted. Poor comparison of the numerical and experimental results only occurs in the stagnation region where high velocity gradients prevail. The turbulent kinetic energy is grossly overpredicted on the jet axis, with the peak computed value being nine times the experimental value, which leads to the prediction of excessive entrainment of the freestream fluid. The prediction improves progressively downstream and by $r/d = 3$ the peak value is within 10% of experiment. The extra entrainment leads to underprediction of the peak radial velocities, which results in the wall jet being too thick. Incorrect values of the individual turbulent stresses will thus be obtained owing to the overprediction of k, since the eddy viscosity concept is used to calculate all the stress components.

Boussinesq's eddy viscosity concept implies that turbulence is isotropic. Inspection of the ratio of the radial to the axial stress components in Figure 6 shows that in the stagnation region the flow is anisotropic, which cannot be accounted for by the numerical model. The anisotropy increases as the impingement plate is approached. On the jet axis, u' reaches twice the value of v' at $y/d = 0{\cdot}25$. This peak occurs for all the radial stations investigated, but reduces in magnitude with distance from the

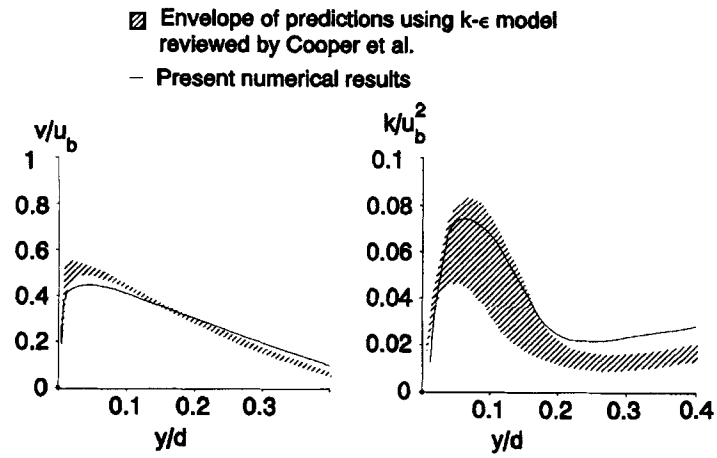

Figure 3. Comparison of predictions with other authors' data

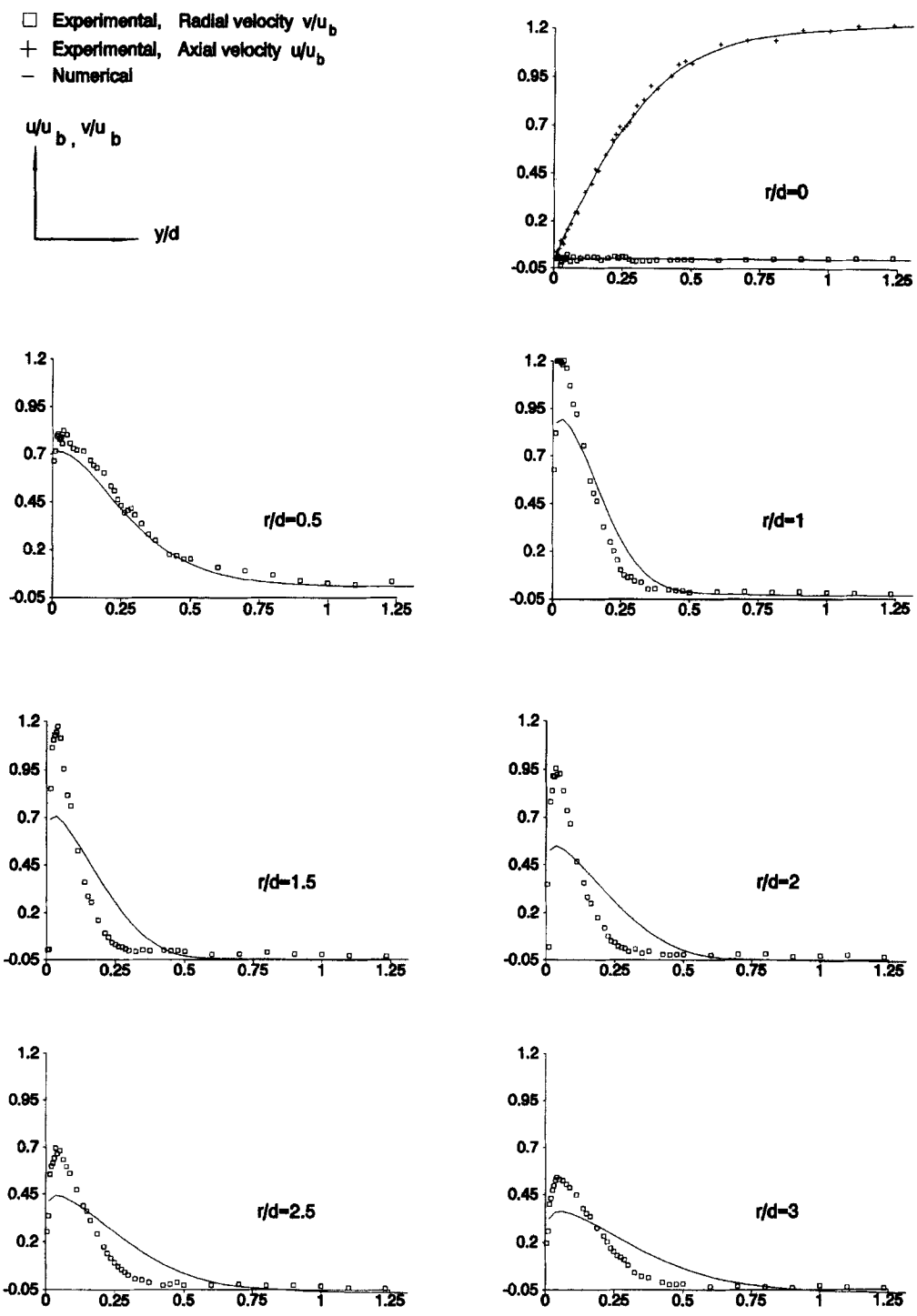

Figure 4. Axial and radial velocity profiles

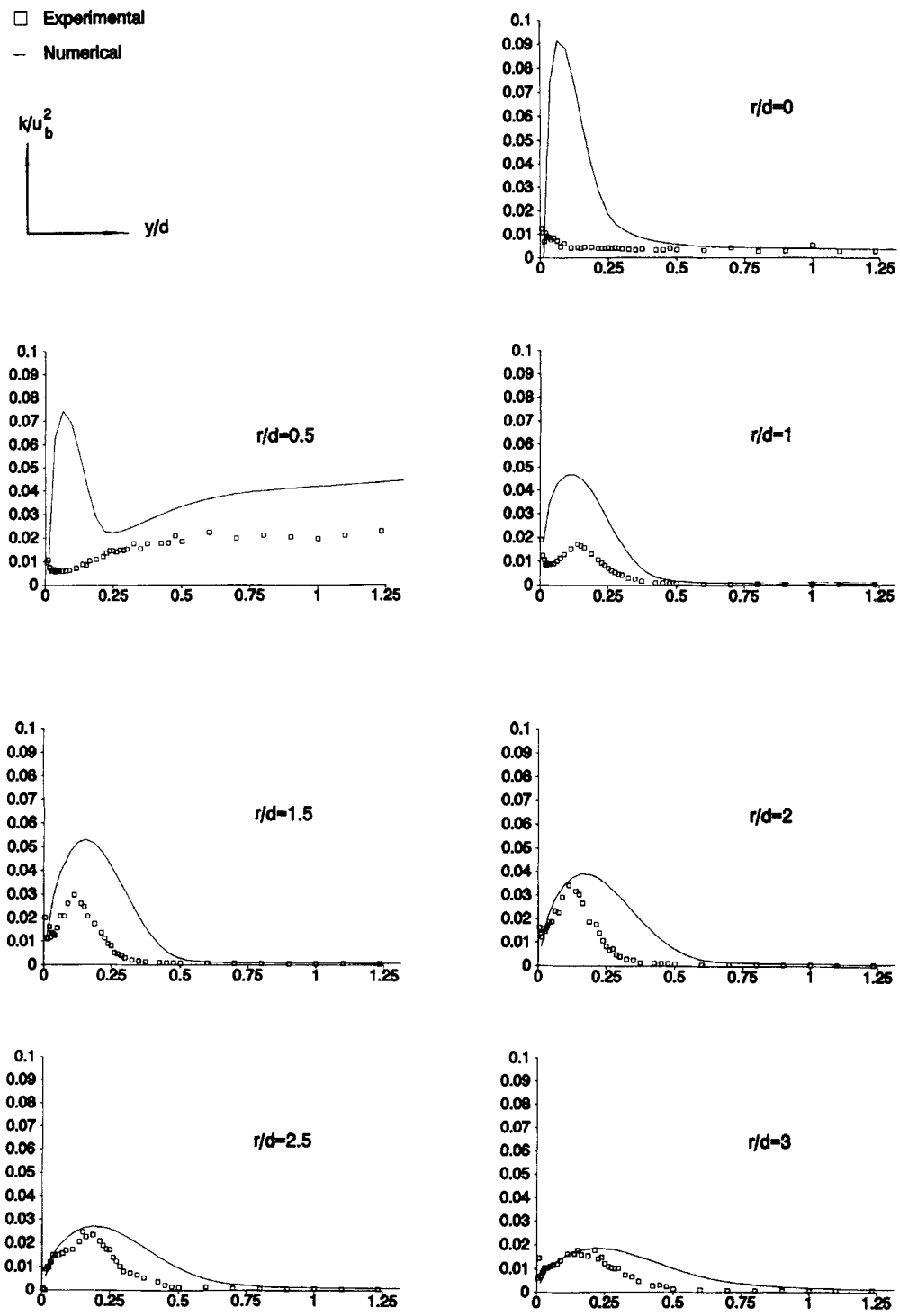

Figure 5. Turbulent kinetic energy

stagnation point. As the wall jet develops and the flow tends to isotropy, the comparison between prediction and experiment improves. In the near-wall region there is a linear relationship between u' and v' typical of boundary layer flow.

4.2. Heat transfer distribution along the plate and the effects of the numerical model

The radial distribution of the computed Nusselt number is compared with experiment in Figure 7. At the stagnation point, *Nu* is overpredicted by over 300%. Comparison between computation and experiment improves with increasing distance from the stagnation point, in line with the improvements in the prediction of k. By $r/d \geqslant 3$ in the wall jet the Nusselt number is predicted to within 20% of the experimental values.

The inability of the numerical model to predict the flow and heat transfer in the stagnation region cannot be attributed solely to the deficiency of the turbulence model in this case. Since $y^+ \sim Re^{0.5}$, a near-wall Reynolds number greater than 132 is required to ensure appropriate use of the wall function. In the present numerical model this condition is only satisfied for $r/d > 0{\cdot}3$, which also corresponds to the location where a significant improvement in the prediction of *Nu* is obtained. It is difficult to specify an appropriate value of y_p for the entire length of a computational domain, especially in a developing flow, without prior knowledge of the flow field. Furthermore, the stagnation region of an impinging jet cannot be compared with a fully developed boundary layer for which the wall function is valid. The radial velocity accelerates rapidly from zero at the stagnation point such that this wall function is inappropriate.

Despite having been developed for two-dimensional flow, the wall function is widely applied to axisymmetric flow. Considering that the developing radial flow in an axisymmetric geometry is moving into a continually enlarging area, it is a reasonable assumption that the flow characteristics in axisymmetric flow will differ from those in a two-dimensional flow. It was demonstrated[32] more than 25 years ago that velocity profiles in axisymmetric flow differ from those in two-dimensional flow and more recently it has been shown[33] that the velocity profile in a pipe flow fails to conform to the accepted law of the wall. These factors will contribute to the 20% difference between the measured and predicted Nusselt numbers in the wall jet obtained in this investigation.

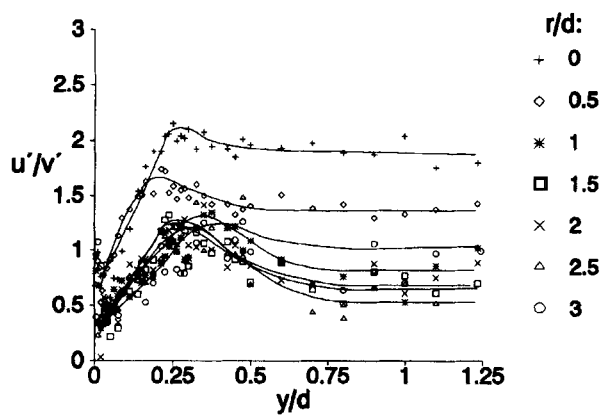

Figure 6. Ratio of normal turbulent stress components

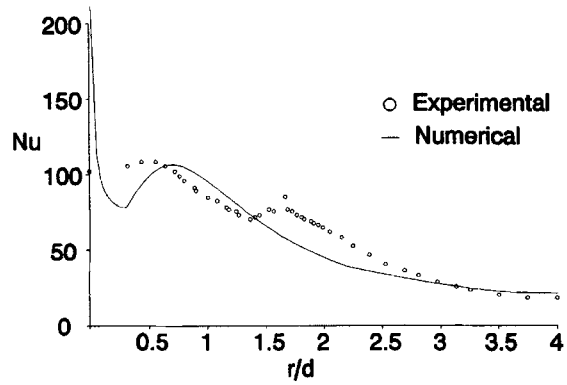

Figure 7. Radial distribution of Nusselt number

Finally, a significant improvement[19] in the prediction of jet impingement using a second-closure approach with new schemes that account for the effect of the wall has been reported. Reasonable comparison of predictions of Nusselt number with experiment for $r/d < 0{\cdot}3$ were obtained. However, an anomaly in the dependence of *Nu* on *Re* at the stagnation point occurred which was attributed to the use of the eddy viscosity concept across the sublayer.

5. CONCLUDING REMARKS

By comparison with other authors' work the commercial CFD package PHOENICS has been shown to predict jet impingement to the same level of accuracy as other available codes that use the same turbulence model.

It has been shown that the widely used k–ε turbulence model can predict the quantitative trends of the radial velocity profiles due to an axisymmetric jet impinging in a semi-confined space, with good quantitative agreement above the wall jet. The qualitative trends of turbulent kinetic energy profiles are also predicted well, except on the axis and at the edge of the jet ($r/d = 0{\cdot}5$) where an overprediction of up to nine times the experimental values occurs. Reasonable quantitative agreement is again shown above the wall jet. For $r/d \geqslant 3$ both the radial velocity and turbulent kinetic energy are fairly predicted (given the numerical and experimental uncertainties) and the comparison improves with radial distance; by $r/d = 3$ the peak values are within 25% and 10% respectively of the experimental results.

The overprediction of turbulent kinetic energy, most significantly in the stagnation region, leads to an underprediction of the spreading rate in the wall jet and to radial velocity profiles that are too thick, although the trends in the wall jet development are predicted.

In the wall jet the heat transfer is predicted to within 20% where the turbulent kinetic energy is reasonably predicted by the k–ε eddy viscosity model and the near-wall nodal spacing meets the requirements of the wall function. However, the stagnation point Nusselt number is overpredicted by about 300%. The prediction of heat transfer improves downstream as the prediction of turbulent kinetic energy improves, which highlights the direct effect of turbulent kinetic energy at the edge of the laminar sublayer on heat transfer. The specification of an inappropriate wall function will also contribute to discrepancies between the results. These factors should be borne in mind when interpreting results from commercial packages.

It is evident that attention needs to be paid to the near-wall predictions. Recent literature has shown that second-moment closures can offer considerable improvement in the prediction of anisotropic flows such that it seems sensible to use a similar approach near the wall, as opposed to the eddy viscosity concept.

Overall, the trends of the jet impingement flow are reasonably predicted and the numerical model can be used with confidence where isotropy prevails and the wall function requirements can be satisfied.

ACKNOWLEDGEMENT

The authors thank the Higher Education Funding Council for financial support towards this work.

APPENDIX: NOMENCLATURE

c_p	specific heat
C_μ, C_1, C_2	turbulence model constants
d	nozzle diameter
h	convective heat transfer coefficient
h_p	enthalpy at near-wall mode
h_w	enthalpy at wall
k	thermal conductivity; turbulent kinetic energy
L	characteristic length scale
Nu	Nusselt number, hd/k
$\dot{q}$	heat flux
r	radial distance from stagnation point
Re	Reynolds number, ud/v
s	skin friction factor
St	Stanton number, $h/\rho c_p v$
u	normal or axial velocity component
u_b	bulk velocity in nozzle
u'	RMS normal velocity; component of normal Reynolds stress
v	radial velocity component
v_p	radial velocity at near-wall node
v'	RMS radial velocity; component of normal Reynolds stress
y	distance from wall
y_p	distance from wall to near-wall node
y^+	non-dimensional distance from wall
z	nozzle-to-plate spacing

Greek letters

ε	dissipation rate of turbulent kinetic energy
κ	von Karman constant
v	kinematic viscosity
ρ	density
$\sigma_k, \sigma_\varepsilon$	turbulence model constants; turbulent Prandtl numbers for diffusion of k and ε
σ_l	laminar Prandtl number
σ_t	turbulent Prandtl number

REFERENCES

1. B. E. Launder, 'Current capabilities for modelling turbulence in industrial flows', *Appl. Sci. Res.*, **48**, 247–269 (1991).
2. B. L. Button and D. Wilcock, 'Impingement heat transfer—a bibliography 1890–1975', *Prev. Heat Mass Transfer*, **4**, 83–89 (1978).
3. B. L. Button and K. Jambunathan, 'Impingement heat transfer—a bibliography 1976–1985', Prev. Heat Mass Transfer **15**, 149–178 (1989).
4. K. Jambunathan and B. L. Button, 'Impingement meat transfer—a bibliography 1986–1993', *Prev. Heat Mass Transfer*, **20**, 385–413 (1994).
5. D. G. Arganbright and H. Resch, 'A review of basic aspects of heat transfer under impinging air jets', *Wood, Sci. Technol.*, **5**, 73–94 (1971).
6. J. N. B. Livingood and P. Hrycak, 'Impingement heat transfer from turbulent air stream jets to flat plates—a literature survey', *NASA TM X-2778*, 1973.
7. Y. Becko, 'Impingement cooling—a review', *von Karman Institute for Fluid Dynamics Lecture Series 83*, 1976.
8. H. Martin, 'Heat and mass transfer between impinging gas jets and solid surfaces', *Adv. Heat Transfer*, **13**, 1–60 (1977).
9. P. Hrycak, 'Heat transfer from impinging jets: a literature review', *AWAL-TR-81-3054, 1981.*
10. S. J. Downs and E. H. James, 'Jet impingement heat transfer—a literature survey,' *ASME Paper 87-H-35*, 1987.
11. S. Polat, B. Huang, A. S. Majumdar and W. J. M. Douglas, 'Numerical flow and heat transfer under impinging jets: a review', *Ann. Rev. Numer. Fluid Mech. Heat Transfer*, **2**, 157–197 (1989).
12. K. Jambunathan, E. Lai, M. A. Moss and B. L. Button, 'A review of heat transfer data for single circular jet impingement', *Int. J. Heat Fluid Flow*, **13**, 106–115 (1992).
13. B. E. Launder, in *Turbulence Modelling for Impinging Flows, ERCOFTAC UK North Pilot Centre/SERC CFD Community Club Workshop*, Manchester, October 1991.
14. J. F. Brison and G. Brun, 'Round normally impinging turbulent jets', *Proc. 15th Meet. of International Association for Hydraulics Research (IAHR) Working Group on Refined Flow Modelling', Lyon, 1991.*
15. J. J. McGuirk, 'A synopsis of the computational results from Lyon/IAHR Workshop', *Proc. European Research Community on Flow Turbulence and Combustion (ERCOFTAC) North Pilot Centre/SERC Community Club*, Manchester, October 1991.
16. J. W. Baughn and S. Shimizu, 'Heat transfer measurements from a surface with uniform heat flux and an impinging jet', *ASME J. Heat Transfer*, **111**, 1096–1098 (1989).
17. D. Cooper, D. C. Jackson, B. E. Launder and G. X. Liao, 'Impinging jet studies for turbulence model assessment—I. Flow field experiments', *Int. J. Heat Mass Transfer*, **36**, 2675–2684 (1993).
18. T. J. Craft and B. E. Launder, 'Comparison of turbulence models in a single impinging jet', in *Turbulence Modelling for Impinging Flows, ERCOFTAC UK North Pilot Centre/SERC CFD Community Club Workshop*, Manchester, October 1991.
19. T. J. Craft, L. J. W. Graham and B. E. Launder, 'Impinging jet studies for turbulence model assessment—II. A comparison of the performance of four turbulence models', *Int. J. Heat Mass Transfer*, **36**, 2685–2697 (1993).
20. S. Ashforth-Frost and K. Jambunathan, 'Effect of nozzle geometry and semi-confinement on the potential core of a turbulent axisymmetric free jet', *Int. Commun. Heat Mass Transfer*, **23**(2), 155–162 (1996).
21. S. Ashforth-Frost, 'Flow visualisation of jet impingement', *Ph.D. Thesis*, Nottingham Trent University, 1994.
22. S. Kline and F. A. McClintock, 'Describing uncertainties in single sample experiments', *Mech. Eng.*, **75**, 3–8 (1953).
23. S. V. Patankar, *Numerical Heat Transfer and Fluid Flow, Hemisphere, New York, 1980.*
24. C. A. J. Fletcher, *Computational Techniques for Fluid Dynamics*, Vol. 1, *Fundamental and General Techniques*, Springer, New York, 1988.
25. C. A. J. Fletcher, *Computational Techniques for Fluid Dynamics*, Vol. 2, *Specific Techniques for Different Flow Categories*, Springer, New York, 1988.
26. J. C. Ludwig, H. Q. Qin and D. B. Spalding, *The PHOENICS Reference Manual, CHAM TR/200*, 1989.
27. S. V. Patankar and D. B. Spalding, 'A calculation procedure for heat, mass and momentum transfer in three dimensional parabolic flows', *Int. J. Heat Mass Transfer*, **15**, 1787–1805 (1972).
28. W. Rodi, *Turbulence Models and Their Application in Hydraulics—A State of the Art Review*, IAHR Section on Division II: Experimental and Mathematical Fluid Dynamics, 1980.
29. B. E. Launder and D. B. Spalding, 'The numerical computation of turbulent flows', *Comput, Methods Appl. Mech. Eng.*, **3**, 269–289 (1974).
30. H. I. Rosten and J. K. Worrell, 'Generalised wall functions for turbulent flow', *PHOENICS J. CFD Appl.*, **1**, 81–109 (1988).
31. C. L. V. Jayatilleke, 'The influence of Prandtl number and surface roughness on the resistance of the laminar sub-layer to momentum and heat transfer, *Prog. Heat Mass Transfer*, **1**, 198–329 (1969).
32. V. C. Patel and M. R. Head, 'Some observations on skin friction and velocity profiles in fully developed pipe and channel flows, *J. Fluid Mech.*, **38**, 181–201 (1969).
33. J. G. M. Eggels, F. Unger, M. H. Weiss, J. Westerweel, R. J. Adrian, R. Friedrich and F. T. M. Nieuwstadt, 'Fully developed turbulent pipe flow: a comparison between direct numerical simulation and experiment', *J. Fluid Mech.*, **268**, 175–209 (1994).